J Mater Sci: Mater Electron (2015) 26:6092–6098
DOI 10.1007/s10854-015-3187-9

Planar microcrystalline ZnO/Si heterojunction photodetector with Al electrodes

Y. M. Hassan[1] · Sh. A. Kakil[1]

Received: 26 January 2015 / Accepted: 9 May 2015 / Published online: 16 May 2015
© Springer Science+Business Media New York 2015

Abstract The fabrication of planar Al/ZnO/Si heterojunction photodetectors has received considerable attention. The crystalline quality of ZnO plays an important role in the properties of the fabricated device. In this study, ZnO micro-rods were grown on Si (100) without any catalysts using atmospheric pressure chemical vapor deposition, and were characterized to determine their potential for application in highly photosensitive ZnO/Si photodetectors. The ZnO rods were grown with various diameters and had a wurtzite structure oriented in the (002) plane. The effect of the substrate temperature on the crystalline structure was studied in the range of 450–750 °C. The planar structure of the Al/ZnO heterojunction photodetector indicated that the device is highly sensitive to ultraviolet and visible light. The photoresponse of the fabricated Al/ZnO device had a peak at 360 nm. The responsivity of the device reached 0.03 at a bias voltage of 1 V and reached 0.085 at a bias voltage of 5 V. The responsivity increased to 0.121 as the bias voltage increased to 10 V. The quantum efficiency of the device was 11, 32, and 42 % at bias voltages of 1, 5, and 10 V, respectively.

1 Introduction

Transparent conducting oxides have been studied extensively because of their broad range of applications such as in transparent electrodes for displays and photovoltaic devices [1, 2]. ZnO has attracted more attention than other transparent conducting oxides because of its large exciton binding energy (60 meV) [3], low resistivity, abundance, and non-toxicity. The optical properties, crystallinity, and the composition of ZnO depend on deposition methods, deposition conditions, and the type of substrate and annealing process [4–7]. The crystal structures of ZnO cubic zinc blend or hexagonal wurtzite make it a promising material for high-speed ultraviolet photodetectors and optical devices [8–11]. A large exciton binding energy suggests that the electron–hole pairs are stable at room temperature and therefore efficient excitonic emission in ZnO can persist at room temperature [12–14].

Various deposition techniques have been developed to fabricate thin layers and lower dimensional structures of ZnO such as rods, belts, tubes, and whiskers. ZnO can form in different crystal shapes depending on the method of deposition, including physical vapor deposition [15], chemical vapor deposition (CVD) [16–18], metal–organic CVD [19], template-assisted growth oxidation method [20], pulsed laser deposition [21], magnetron sputtering [22, 23], and sol–gel methods [24]. Despite the adaptation of some approaches to ZnO growth, the control of the size, shape, crystallinity, and the parameters that affect the growth still need more investigation.

Narrow-band gap semiconductors are usually used for ultraviolet (UV) detection because they exhibit high gain and low noise and they can be visible-blind. The disadvantage of these devices is their sensitivity to low energy radiation, which results in a significant loss of the effective area of the device. This has promoted some researchers to use wide direct band gap materials to fabricate optoelectronic devices that are sensitive in the UV region. ZnO is a semiconductor with a wide direct band gap that is sensitive in the UV region. It is of low cost and is easy to fabricate. The ZnO/Si heterojunction recently has received attention

✉ Y. M. Hassan
yousif.60@hotmail.com; yousif.60@uni-sci.org

[1] Department of Physics, College of Science, Salahaddin University, Erbil, Kurdistan, Iraq

because it has a low driving voltage and is inexpensive to fabricate. Important results on ZnO/Si heterojunction metal–semiconductor–metal photodetectors have been previously reported [25, 26].

The purpose of the present work is to prepare ZnO microstructures on the surface of *p*-type (100) substrates without any catalysis, and to study the effect of the substrate temperature on the grown ZnO. Morphology, crystalline structure, and elemental composition of the grown ZnO microrods were investigated. The ZnO crystalline rods formed at 650 °C were used to fabricate Al/ZnO/*p*-Si (100) heterojunctions. The photoelectrical properties of the photodetectors such as current–voltage (I–V) characteristics, photoconductivity, photoresponse, and sensitivity were studied.

2 Experimental details

An atmospheric pressure chemical vapor deposition APCVD system was used to form the ZnO films. The system had a horizontal quartz reactor of diameter 70 mm equipped with different accessories such as heating systems and control systems for the gas supply tubes. The temperature profile inside the quartz tube was carefully determined prior to the growth of the ZnO. The silicon substrate surfaces were cleaned using a standard Radio Corporation of America (RCA) cleaning method and dried by blowing Ar. The substrates were loaded on the susceptor, which was fixed at 45° in the reactor tube. The ZnO products were deposited on *p*-type Si (100) in one run or different runs with the same deposition conditions. During the deposition process, $ZnCl_2$ was evaporated at temperature of ~480 °C at 5 cm away from the susceptor. The gas flow rate ratio $ZnCl_2/O_2 = 1$ and substrate temperature was kept constant during the deposition process.

The morphology of ZnO products was studied using field emission scanning electron microscopy (FESEM). The phase identification of the ZnO crystal was carried out using X-ray diffraction (XRD) profiles, collected using an X-ray system (Rigaku, D/MAX-Rc) at a wavelength of 0.154 nm. Energy dispersive X-ray spectroscopy (EDX, LeoSupra50VP) was used to identify the composition of the ZnO products. The ZnO/Si heterojunction structure was prepared at a substrate temperature of 650 °C. This heterojunction was used for fabrication of the planar Al/ZnO photodetector with interdigitated top contacts. A monochromatic UV light of wavelength $\lambda = 320$ nm was used to illuminate the photodetector. A monochrometer of type MP-1018B was used to measure the spectral response.

3 Results and discussion

3.1 XRD of ZnO/Si structures

Figure 1 shows four XRD patterns of the grown ZnO crystal rods on Si at different substrate temperatures. Figure 1a shows the diffraction pattern of the crystal rods prepared at 450 °C. There were several diffraction peaks at the (100), (002), (101), (102), (110), and (200) crystal planes. These peaks were assigned to hexagonal wurtzite and belong to the space group P63mc (see Table 1). The XRD patterns did not change significantly when substrate temperatures of 550 and 650 °C were used, except there was an increase in the peak intensity at the (100), (002), and (101) planes (see Fig. 1b, c). When the substrate temperature was increased to 750 °C, new peaks appeared. These peaks are marked by the red stars (*) in Fig. 1d. These peaks were assigned to Zn_2SiO_4 compounds, consistent with Joint Committee on Powder Diffraction Standards (JCPDS) card No. 13597-65-4. The formation of Zn_2SiO_4 at the interface of ZnO and Si is important in many advanced optoelectronic applications such as solid-state white lighting and flat panel display devices.

The lattice parameter (c), crystal strains (ε), and bond lengths (L) of grown ZnO on Si at different substrate temperatures were calculated and are recorded in Table 1. The interplanar spacing (d) values and diffraction angles are in good agreement with the standard data of bulk ZnO. It was found that the (002) peak slightly shifted from 34.4157° to 34.4205° when increasing the deposition temperature from 450 to 650 °C because of the relaxation of the crystal strain. The crystal strain can be calculated using:

$$\varepsilon = \frac{c - c_0}{c_0} \times 100$$

The bond length (L) was calculated using:

$$L = \sqrt{\left[\frac{a^3}{3} + \left[\frac{1}{2} - u^2\right]^2 c^2\right]},$$

where the parameter u for the wurtzite structure is given by

$$u = \frac{a^2}{3c^2} + 0.25.$$

The values of c, d, strains, and bond lengths of the ZnO on Si substrate prepared at a substrate temperature of 450–750 °C remained constant and were close to the standard values for crystalline ZnO. The slightly high values of the crystal parameters for the ZnO/Si sample prepared at 750 °C is related to production of a new compound (Zn_2SiO_4) in the product, detected using XRD.

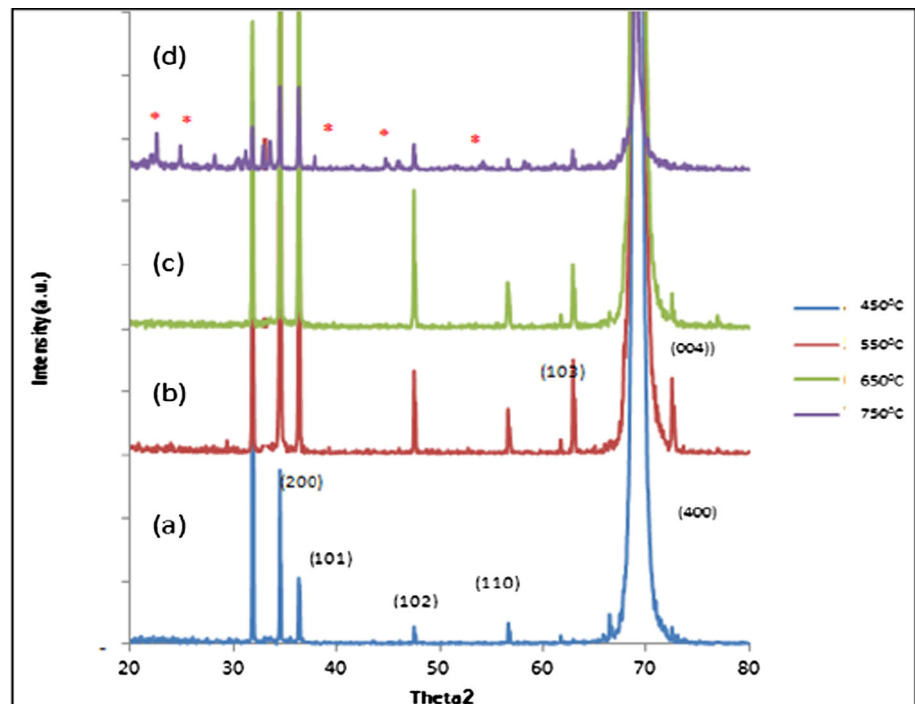

Fig. 1 XRD diffraction pattern of ZnO/Si crystal at different susbtrate temperatures

Table 1 Lattice parameter (*c*), strains and bond lengths of grown ZnO on Si at different substrate temperatures

Ts/°C	d (Å)	c (A) (002)	$\varepsilon \times 10^3$	L (Å)
450	2.60435	5.2087	0.34	1.3021
550	2.60377	5.2075	0.11	1.3018
650	2.60359	5.2071	0.012	1.3017
750	2.60558	5.2097	0.553	1.3029

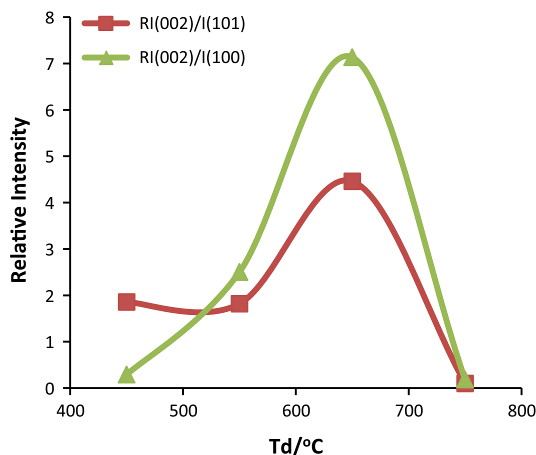

Fig. 2 The ratio of relative intensity of RI (002)/I (100) and RI (002)/I (101) peaks versus deposition temperature for ZnO/Si

A plot of the ratio of relative intensity [RI (002)/I (100) and RI (002)/I (101)] of the XRD peaks against growth temperature for ZnO/Si structure, is shown in Fig. 2. It is clear that RI (002)/I (100) and RI (002)/I (101) increased with increasing substrate temperature between 450 and 650 °C. The predominant ZnO (002) peak on the Si substrate can be related to spontaneously grown SiO_2 on Si during the growth of ZnO/Si. The decrease in intensity for RI (002)/I (100) and RI (002)/I (101)when the substrate temperature was increased between 650 and 750 °C is because of the formation of a new phase of Zn_2SiO_4 during the growth of ZnO at substrate temperatures higher than 650 °C.

3.2 FESEM analysis

Figure 3a shows an FESEM image of ZnO on a Si substrate grown at a temperature of 450 °C. This image shows that there was a low number of microrods per selected unit area with rod diameters in range of 650–700 nm. When the deposition temperature increased to 550 °C, the number of rods per unit area increased and the shape of the crystals mostly remained hexagonal. Figure 3b shows the FESEM image of ZnO on Si grown at a temperature of 650 °C. This image shows that the number of rods per unit area with rod diameters in the range of 300–600 nm increased and had different crystal shapes. The cross-sectional SEM image of

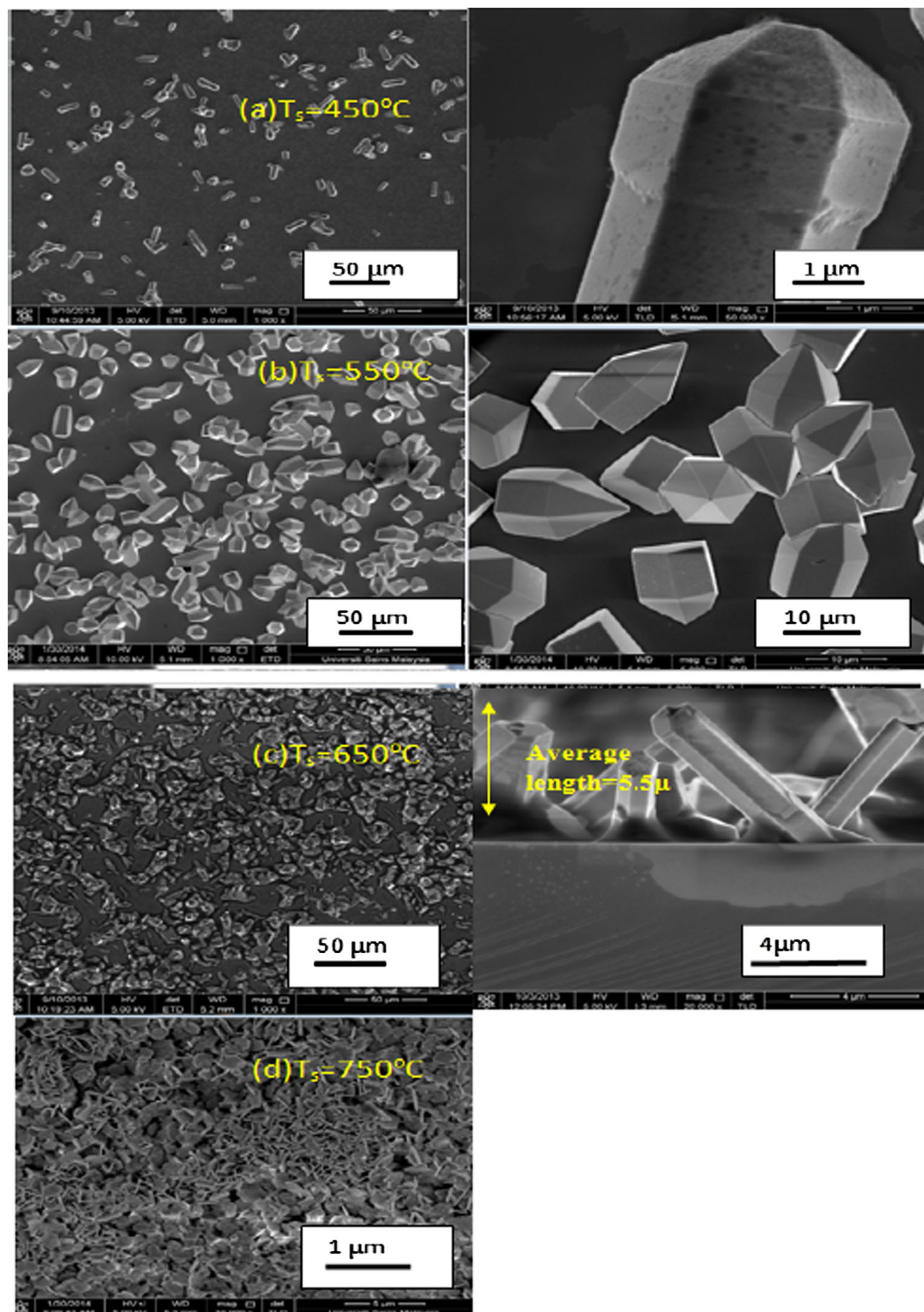

Fig. 3 Surface FESEM images of ZnO structure on *p*-Si substrate **a** grown at temperature 450 °C, the right image shows the enlarged SEM image of a single ZnO crystal. **b** Grown at temperature 550 °C, the right image shows the enlarged SEM image of a number ZnO crystals. **c** grown at temperature 650 °C with Cross-sectional FESEM image. **d** Grown at temperature 750 °C

this sample is shown on the right. This image shows that ZnO rods grown on Si had an average length of about ~5.5 µm and were oriented in different directions. Figure 3c shows the FESEM image of ZnO grown on Si at a temperature of 750 °C. As the number of rods increased and the rod diameter decreased to the range of 100–300 nm, the shape of the crystals remained hexagonal with the appearance of some prism-like shapes. It is suggested that increasing the deposition temperature results in decreasing the ZnO rod sizes. This is owing to the decrease of the mismatch between the Si and ZnO products because of spontaneous growth of SiO_2 during the deposition

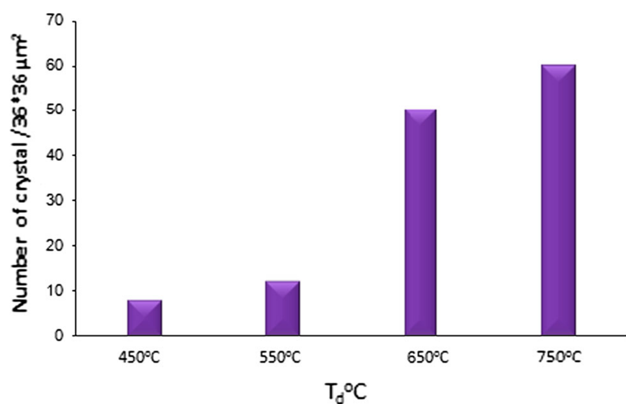

Fig. 4 Number of ZnO crystals per unit area versus substrate temperatures

process of the ZnO product, which starts to produce a thin ZnO film.

The number of ZnO crystals per unit area on the Si substrate at different substrate temperatures is presented as a histogram (Fig. 4). The histogram shows that the number of rods per unit area increased with increasing substrate temperature. According to the FESEM images, the rod diameters decreased from 600 to 100 nm.

3.3 EDX analysis

Figure 5 shows the EDX profile of ZnO/Si structure prepared at 650 °C. The O and Zn peaks were at 0.5 and 1 keV, respectively. The Zn/O ratio of 1.141 confirms that the ZnO crystals at this temperature were highly crystalline.

It was found that Zn/O ratio increased with increasing deposition temperature as shown in the inset of Fig. 5. This means the crystal quality improved.

3.4 Photoelectric properties

The planar Al–ZnO/Si heterojunction photodetectors consist of two interdigitated Schottky contacts (“fingers”) deposited on top of the ZnO layer as shown in Fig. 6a. The current–voltage (I–V) characteristics of the planar Al/ZnO microrod photodetector with and without UV illumination (189 µW at 320 nm) are shown in Fig. 6b. The I–V curves were measured using a bias of −10 to 10 V at room temperature. The dark I–V curve of the Al/ZnO photodetector measured at a low forward voltage of <4 V had a current that was linearly dependent on the applied voltage. This is because of the good Ohmic contact between ZnO and the electrodes. However, at a forward voltage of >4 V, the current passes through a thin ZnO layer and the avalanche multiplication process occurs to generate a large number of carriers. The space charge region at the ZnO/Si interface, which includes the entire ZnO layer and extends into the Si substrate, has a high barrier resulting in high number of accumulated carriers. This increases recombination and thus few carriers are generated from the avalanche multiplication process [27].

To understand the UV-illuminated I–V behavior of Al/ZnO photodiodes, the energy band diagram of the ZnO/Si

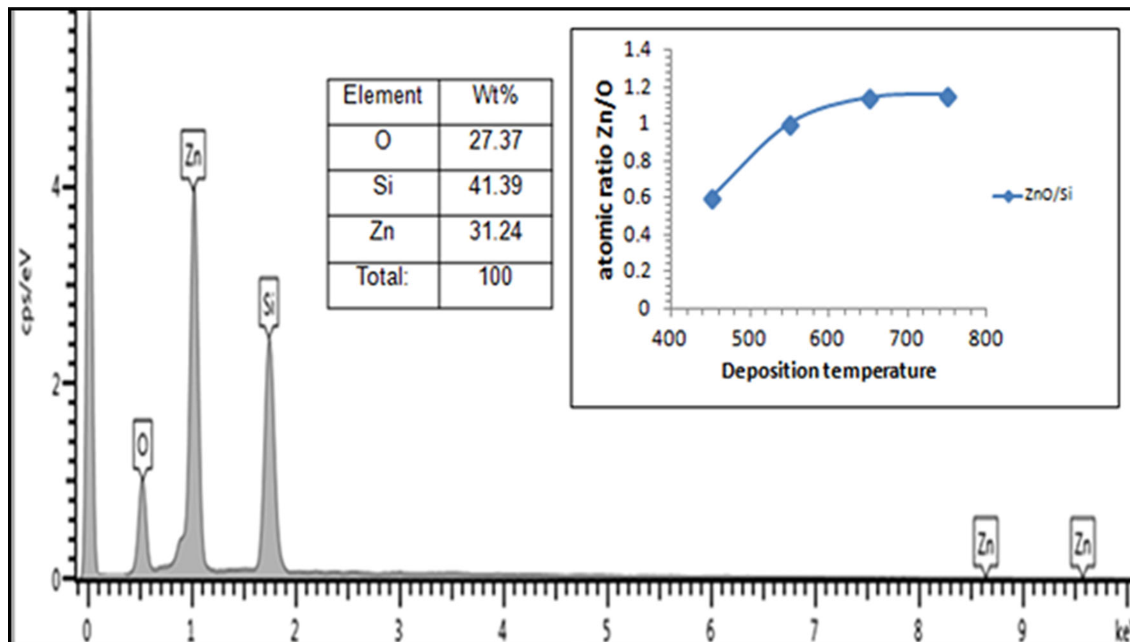

Fig. 5 EDX spectrum of ZnO/Si structure prepared at substrate temperature 650 °C. The inset shows the increase of Zn/O ratio with substrate temperature

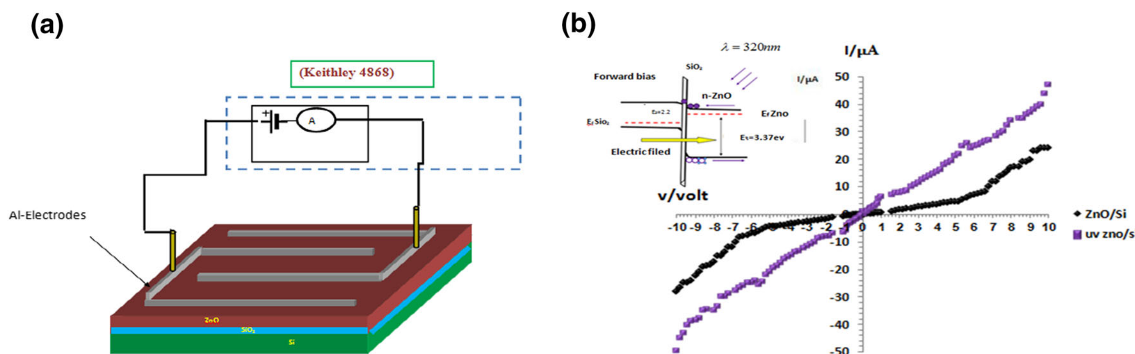

Fig. 6 **a** A planar Al/Zn/Si Photo detector on Si substrate. **b** *Dark* and UV illuminated I–V of the Al/ZnO/Si photodetectore (the band diagrams of ZnO/Si hetrojunctions depicted in the *inset* of (**b**)

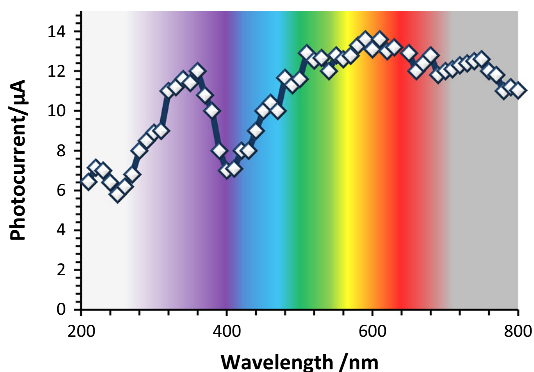

Fig. 7 Spectral photocurrent of planar Al/ZnO/Si photodetector at 5 V

heterojunction is shown in the inset of Fig. 6. Under forward bias, photogenerated electrons in the space charge region of the ZnO/Si can tunnel through the barrier and the photogenerated holes drift to the ZnO side, resulting in a high photoelectric signal.

Under reverse bias, there are photogenerated minority electrons in the depleted Si region and photogenerated holes in the depleted *n*-type ZnO region. The current can pass through the barrier owing to the strong external electric field. The photocurrent is composed of both the majority carriers and the minority carriers and is the same order of magnitude as the photocurrent of the device at a forward bias.

Figure 7 shows the photocurrent spectrum for the planar Al/ZnO/photoconductor. The device photoresponse started at 200 nm and reached its peak value at around 365 nm. This peak value corresponds to the band gap of ZnO. The photocurrent clearly dropped at around a wavelength of 400 nm because of traps at ZnO/Si interface, the photocurrent started to increase from 400 to 800 nm owing to the absorption of the transmitted part of the spectrum through the ZnO layer by Si, which produces a photocurrent in the visible range.

The responsivity (R) is defined as the ratio of the measured photoresponse to the incident optical power on the UV photodiode. Table 2 shows the recorded responsivity values for some planar MSM photodetectors published in literature with their bias voltages. The high responsivity for our device (0.112 A/W) at a bias voltage of 7 V is because of the increase in avalanche processes and the carrier acceleration by the electric field on the ZnO microrods.

The sensitivity of planar Al/ZnO photodetectors was measured as function of the forward bias voltage (0–10 V) and the results are shown in Fig. 8. It is clear that the sensitivity of this device is high at low bias voltages and decreased with increasing bias.

The optical to electrical conversion efficiency of the photodiode, the external quantum efficiency (η), was

Table 2 Responsivity of planar Al/ZnO photodetectors compared with the results reported on planar ZnO photodetectors in the literature

Configuration	λ (nm)	Voltage (V)	R (A/W)	References
Al/ZnO/Si	320	1, 5, 7	0.030, 0.085, 0.112	This work
Au/Cr/ZnO/SiO2/Al	365	3	0.056	[28]
Pd/ZnO/PSi/Pd	300–380	5	0.22	[29]
Pd/ZnO/quartz/Pd	300–380	5	0.073	[29]
Pd/ZnO/Si/Pd	365	5	0.09	[29]
Ag/ZnO/PSi/Ag	325	5	0.101	[30]
Ag/ZnO/Ag	370	1	0.066	[31]

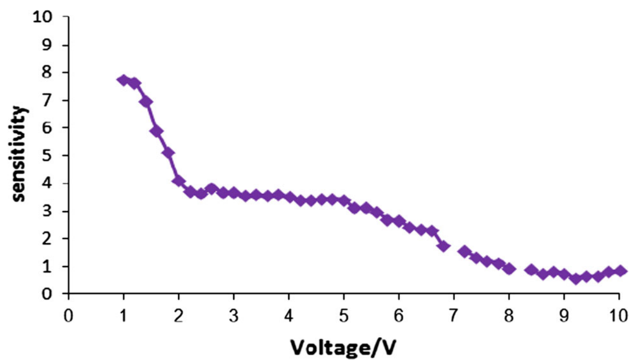

Fig. 8 Sensitivity of planar Al/ZnO/Si photodetector as a function of applied voltage under

determined by measuring the spectral response [32]. The values of the quantum efficiency of the Al/ZnO photodetectors were 11, 31.867, and 42 % at a voltage bias of 1, 5, and 10 V, respectively. These values are high when compared with the values reported in the literature [29].

4 Conclusions

ZnO microcrystal rods were successfully grown on the Si (100) substrates using APCVD at various substrate temperatures ranging from 450 to 750 °C. The influence of the substrate temperature on the structural of ZnO products was studied. The XRD measurements showed that the products deposited at 650 °C have a preferential orientation in the (002) direction, with a minimum FWHM value of 0.2952°. This indicates that the crystallinity of the products improved. The formation of crystalline Zn_2SiO_4 at the interface of ZnO and Si is reported. The FESEM images of the ZnO products showed that the number of ZnO crystals per selected unit area increased with increasing deposition temperature and that most crystals had a hexagonal shape. EDX analysis showed that the atomic ratio Zn/O in the products increased with increasing deposition temperature. The planar Al/ZnO microrod/Si heterostructure UV photodetector was fabricated. Under UV illumination of 320 nm, the device showed a good responsivity and a high quantum efficiency at a high bias voltage with a high sensitivity at a low bias voltage.

Acknowledgments The authors gratefully acknowledge the support from Department of Physics, College of Science at the University of Slahaddin. The authors are also grateful to Dr. Naser M. Ahmed Al-rawi for assistance with the FESEM, EDX, and XRD measurements.

Conflict of interest The authors declare that they have no conflict of interest.

References

1. M. Chen, Z.L. Pei, C. Sun, J. Gong, R.F. Huang, L.S. Wen, Mater. Sci. Eng. B **85**, 212 (2001)
2. J. Herero, M.T. Gutierrez, C. Guillen, J.M. Dona, M.A. Martinez, A.M. Chaparro, Thin Solid Films **361–362**, 28 (2000)
3. V. Srikant, D.R. Clarke, J. Appl. Phys. **83**, 5447 (1998)
4. H. Kim, J.Y. Moon, H.S. Lee, Curr. Appl. Phys. **12**, S35 (2012)
5. L.S. Chuah, Z. Hassan, S.S. Tneh, H. Abu Hassan, Compos. Interfaces **17**(8), 733 (2010)
6. H. Hou, Y. Xie, Q. Li, Solid State Sci. **7**(1), 45 (2005)
7. A.K. Zak, M.E. Abrishami, W.H. Abd Majid, Ceram. Int. **37**, 393 (2011)
8. H.D. Um, S. Abdul Moiz, K.T. Park, J.Y. Jung, S.W. Jee, C.H. Ahn, D.W. Kim, H.K. Cho, D.W. Kim, J.H. Lee, Appl. Phys. Lett. **98**, 033102 (2011)
9. S.W. Kim, S. Fujita, Appl. Phys. Lett. **81**, 5036 (2002)
10. X.W. Sun, H.S. Kwok, J. Appl. Phys. **86**, 408 (1999)
11. J.S. Liu, C.X. Shan, H. Shen, B.H. Li, Z.Z. Zhang, L. Liu, L.G. Zhang, D.Z. Shen, Appl. Phys. Lett. **101**, 011106 (2012)
12. S.K. Panda, C. Jacob, Solid State Electron. **73**, 44 (2012)
13. J.G. Lu, T. Kawaharamura, H. Nishinaka, Y. Kamada, T. Ohshima, S. Fujita, J. Cryst. Growth **299**, 1 (2007)
14. N. Takahashi, K. Kaiya, K. Omichi, T. Nakamura, S. Okamoto, H. Yamamoto, J. Cryst. Growth **209**, 822 (2000)
15. T. Terasako, S. Shirakata, Jpn. J. Appl. Phys. **44**, 1410 (2005)
16. K.T. Roro, J.K. Dangbegnon, S. Sivaraya, A.W.R. Leitch, J.R. Botha, J. Appl. Phys. **103**, 053516 (2008)
17. T. Singh, D.K. Pandya, R. Singh, J. Nano- Electron. Phys. **3**(1), 146 (2011)
18. T. Ohshima, R.K. Thareja, T. Ikegami, K. Ebihara, Surf. Coat. Technol. **169**, 517 (2003)
19. T.K.S. Naidu, B. Srinivasulu, S. Uthanna, Cryst. Res. Technol. **35**(10), 1193 (2000)
20. S.W. Rhee, H.W. Choi, Trans. Electr. Electron. Mater. **14**(2), 86 (2013)
21. Z.R. Khan, M.S. Khan, M. Zulfequar, M.S. Khan, Mater. Sci. Appl. **4**, 340 (2011)
22. V.V.S. Kumar, F. Singh, S. Ojha, D. Kanjilal, Adv. Mater. Lett. **4**(5), 343 (2013)
23. R. Sing, M. Kumar, S. Chandra, J. Mater. Sci. **42**(12), 4675 (2007)
24. A. Drici, G. Djeteli, G. Tchangbedji, H. Derouiche, K. Jondo, K. Napo, J.C. Berne‘de, S. Ouro-Djobo, M. Gbagba, Physica Status Solidi (a) **201**(7), 1528 (2004)
25. Z. Bai, X. Yan, X. Chen, H. Liu, Y. Shen, Y. Zhang, Curr. Appl. Phys. **13**, 165 (2013)
26. Z. Bai, X. Yan, X. Chen, Y. Cui, P. Lin, Y. Shen, Y. Zhang, RSC Adv. **3**, 17682 (2013)
27. T. Yen, J. Yun, S.J. Kim, Electrochem. Solid-State Lett. **14**, H415 (2011)
28. G.M. Ali, P. Chakrabarti, J. Phys. D Appl. Phys. **43**, 415103 (2010)
29. H.I. Abdulgafour, Z. Hassan, N.M. Ahmed, F.K. Yam, J. Appl. Phys. **112**, 074510 (2012)
30. M. Rajabi, R.S. Dariani, A. IrajiZad, Sens. Actuators A **180**, 11 (2012)
31. S.J. Young, L.W. Ji, S.J. Changa, Y.K. Su, J. Cryst. Growth **293**, 43 (2006)
32. G.M. Ali, P. Chakrabarti, J. Phys. D Appl. Phys. **43**(41), 415103 (2010)